PHYSICAL REVIEW B **90**, 054305 (2014)

Wave propagation in twisted metamaterials

Amir Nader Askarpour, Yang Zhao, and Andrea Alù*

Department of Electrical and Computer Engineering, The University of Texas at Austin, 1 University Station C0803, Austin, Texas 78712, USA

(Received 24 June 2014; revised manuscript received 4 August 2014; published 25 August 2014)

Twisted metamaterials, or arrays of identical planar metasurfaces stacked with a sequential rotation, have been recently introduced to realize broadband circular dichroism. Here we develop a generalized Floquet analysis to obtain the exact modal solutions for eigenwaves supported by these structures. The dispersion relation and wave propagation in twisted metamaterials are discussed in detail. Our analysis shows how the modal dispersion in these metamaterials becomes inherently different from the one of conventional periodic structures and how the eigenmodes support specific circular polarization properties based on a lattice effect, even when achiral inclusions are considered. These wave properties are ideal to realize optical devices that manipulate the polarization state of light over broad bandwidths. By analyzing the physical nature of these modes, including complex modes, we also extend the application of twisted metamaterials to realize passband and stop-band nanophotonic structures with strong polarization manipulation properties.

DOI: 10.1103/PhysRevB.90.054305 PACS number(s): 41.20.Jb, 42.25.Bs, 42.25.Ja, 42.25.Lc

I. INTRODUCTION

Introducing a sequential rotation in an otherwise periodic array results in new possibilities for manipulating and engineering wave propagation. These twisted arrays of particles are the building blocks of nematic liquid crystals and of a range of newly developed metamaterials with applications to negative refractive index and partial focusing [1–7], perfect lenses [8], broadband polarizers [9], optically active media [10–16], polarization rotators [17], enhanced reflectors [18], unidirectional optical waveguides [19], photonic crystals [20,21], chromatic aberration correctors [22], giant chirality [23], and superchiral light [24,25]. Twisted structures have also been recently studied to improve the performance of high-power microwave sources [26–28] in which a waveguide with helical grooves is used to boost the interaction between electromagnetic waves and electron beams. The same concept can be used to obtain circular dichroism in optical waveguides [29,30]. Since the twisted arrays have different structural symmetries compared to conventional periodic arrays, the methods developed to obtain modal solutions of periodic arrays [31–34] are not directly applicable to twisted metamaterials. To study the wave phenomena in twisted structures, ranging from twisted chains of nanoparticles to three-dimensional (3D) models of liquid crystals, various methods have been applied in the literature, including geometrical optics [35,36], coupled-mode theory [37,38], Riccati's equation modeling [39], finite element methods [40], Green's function methods [31–42], and the transfer-matrix methods [43–52].

Among these techniques, the transfer-matrix method has several advantages in terms of rigorousness, speed, and analytical simplicity. This technique assumes that the medium is composed of multiple anisotropic layers with a sequential rotation [52] and each layer is represented by a 4×4 transfer matrix so that by cascading the individual matrices, the collective response of the material may be found. This method is especially useful when dealing with a small number of layers; however, it becomes impractical when the array becomes large.

Here, based on this approach, we introduce a generalized Floquet formalism to study the eigenmodes supported by a 3D twisted metamaterial, consisting of an infinite array of identical metasurfaces rotated sequentially along the array axis [9]. After deriving the normal modes supported by the array, which are orthogonal to each other, we express the fields inside the stratified twisted metamaterial using a superposition of left- and right-handed circularly polarized plane waves. This analysis helps us highlight the wave propagation properties in these structures and provide additional insight into their eigenmodal propagation properties. Our results show that twisted metamaterials can support eigenmodes with strong circular polarization properties as well as complex eigenmodes that, although not being excited by plane waves impinging from free space, may affect the evanescent spectrum and local density of states near a slab of twisted metamaterials. It is worth mentioning that the theory developed for analyzing waveguides with step and turn symmetry [30] can be considered as a special case of the results presented in the following. In the next section, we introduce our analysis to model a twisted array of metasurfaces and discuss the general properties of these solutions. Throughout this paper, we assume an $e^{-i\omega t}$ time dependence.

II. EIGENSOLUTION FOR TWISTED METAMATERIALS

A unit cell in the transverse direction for a twisted metamaterial, consistent with the geometry originally introduced in Ref. [9], is shown schematically in Fig. 1. The parallel metasurfaces consist of periodic repetitions in the x-y directions of the inclusions shown in Fig. 1, and they are assumed to reside in constant-z planes with a negligible thickness. The distance d between neighboring metasurfaces is assumed constant through the array. Each metasurface is indexed using an integer number n with $n = 0$ placed at the $z = 0$ plane. The twist is obtained by rotating each metasurface by a constant angle θ with respect to its immediate neighbor. Therefore, the nth metasurface is rotated by $n\theta$ radians and is translated by nd along the z direction, compared to the 0th

*alu@mail.utexas.edu

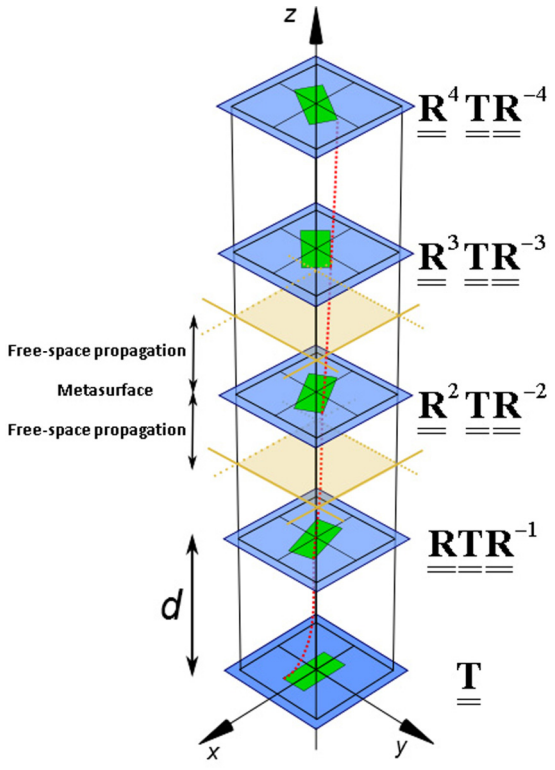

FIG. 1. (Color online) Schematic geometry of a twisted metamaterial. Each layer is rotated by a constant angle compared to its immediate neighbor. The transfer matrix of each twisted unit cell can be obtained by suitably rotating the transfer matrix of the first unit cell. A twisted unit cell consists of a propagation length d in free space and an ultrathin metasurface in the middle.

metasurface. In the following analysis, the twist angle θ can be chosen arbitrarily as long as it is kept constant throughout the structure.

We construct the "twisted unit cell" of the metamaterial by sandwiching the transfer matrix of the generic metasurface between the two transfer matrices of free-space segments with equal lengths $d/2$ as shown in Fig. 1. If $\underline{\underline{\mathbf{T}}}$ is the transfer matrix of a metasurface, the transfer matrix of a twisted unit cell can be written as $\underline{\underline{\mathbf{R}}}\underline{\underline{\mathbf{T}}}\underline{\underline{\mathbf{R}}}^{-1}$, where $\underline{\underline{\mathbf{R}}}$ is the 4×4 rotation matrix [53] (see the Appendix for the expression of these tensors). Therefore, the fields that enter the $(n+1)$-th twisted unit cell can be written as a function of the fields at the nth twisted unit cell as

$$\mathbf{f}_{n+1} = \underline{\underline{\mathbf{R}}}^n\underline{\underline{\mathbf{T}}}\underline{\underline{\mathbf{R}}}^{-n}\mathbf{f}_n, \tag{1}$$

where $\mathbf{f}$ is a 4×1 vector containing the transverse components of both electric and magnetic fields. The generalization of Floquet's theorem for this twisted structure requires defining generalized eigenmodes that are self-sustained as they propagate through the twisted unit cells. The eigenvectors need to satisfy the symmetry condition [55],

$$\mathbf{f}_{n+1} = \underline{\underline{\mathbf{R}}}e^{i\beta d}\mathbf{f}_n, \tag{2}$$

where β is the complex wave number in the twisted array. Equation (2) describes the fields at the input of any twisted unit cell as a rotated and phase-shifted replica of the fields at the input of the next unit cell, illustrated by the dotted red curve in Fig. 1. From Eqs. (1) and (2), the following eigensystem can then be derived:

$$(\underline{\underline{\mathbf{R}}}^n\underline{\underline{\mathbf{T}}}\underline{\underline{\mathbf{R}}}^{-n} - \underline{\underline{\mathbf{R}}}e^{i\beta d})\mathbf{f}_n = 0. \tag{3}$$

It can be readily proved using mathematical induction that if a wave number satisfies the above equation for a specific integer n, it will also satisfy the equation for all other integer values of n. This shows that the derived eigensystem is self-consistent, and the generalized eigenmodes defined in (2) can be supported by the twisted metamaterial. Since β is independent of n, we can solve Eq. (3) for $n = 0$ and find all supported wave numbers.

In general, the eigenvalue problem (3) results in a fourth-order equation with four distinct eigenvalues, two of which correspond to modes propagating in the positive direction and the other two in the negative direction. It should be stressed that one cannot determine the direction of propagation by simply considering the sign of the propagation constant because of the involved field rotation at each twisted unit cell. The appropriate direction of propagation may be found by considering a small amount of loss in each metasurface and examining the decay direction of the eigenmodes or equivalently by computing the power flow direction for each eigenmode as we do in the next section.

We show in the Appendix that, for each forward mode solution ($\mathbf{E}$, $\mathbf{H}$, and β) of (3) in a time-reversal symmetric twisted metamaterial, there will be also a mode propagating in the opposite direction with a similar wave number ($\mathbf{E}^*$, $-\mathbf{H}^*$, and $-\beta^*$). Thus, solutions to (3) can be limited to positive propagation constants in a reciprocal metamaterial, and the corresponding dispersion equation is an even function of the propagation constant. By generalizing the results in Ref. [56], we can also show that the eigenmodes supported by the twisted metamaterial are orthogonal to each other. Therefore, it is possible to induce each mode independently with proper excitation, and they carry power without mutual coupling, despite the rotation and polarization couplings in the system.

Another relevant property of twisted metamaterials that arises from symmetry considerations, also formally derived in the Appendix, is that two arrays with the same metasurfaces and opposite rotation angle θ have the same propagation properties. A forward propagating mode ($\mathbf{E}$, $\mathbf{H}$, and β) in one metamaterial corresponds to a mode propagating in the opposite direction ($\mathbf{E}$, $-\mathbf{H}$, and $-\beta$) in the other one, a simple consequence of the fact that a right-handed structure is transformed into a left-handed structure after mirror symmetry. For reciprocal arrays this implies that, by changing the sense of rotation of the array, the sense of rotation of the fields is also flipped. In mathematical terms, if $\mathbf{E}$ and $\mathbf{H}$ are eigenmodal solutions with wave number β for a twisted metamaterial with positive rotation, then the solution for negative rotation can be written as $\mathbf{E}^*$, $\mathbf{H}^*$ with wave number β^*.

In order to understand the modal properties of twisted metamaterials, we analyze a simple geometry consisting of arrays of perfectly electric conducting (PEC) rods. We choose this geometry because each inclusion does not support any intrinsic chiral response or polarization coupling, allowing us to better highlight the effects of the lattice rotation on the propagating modes. In our example, each metasurface is

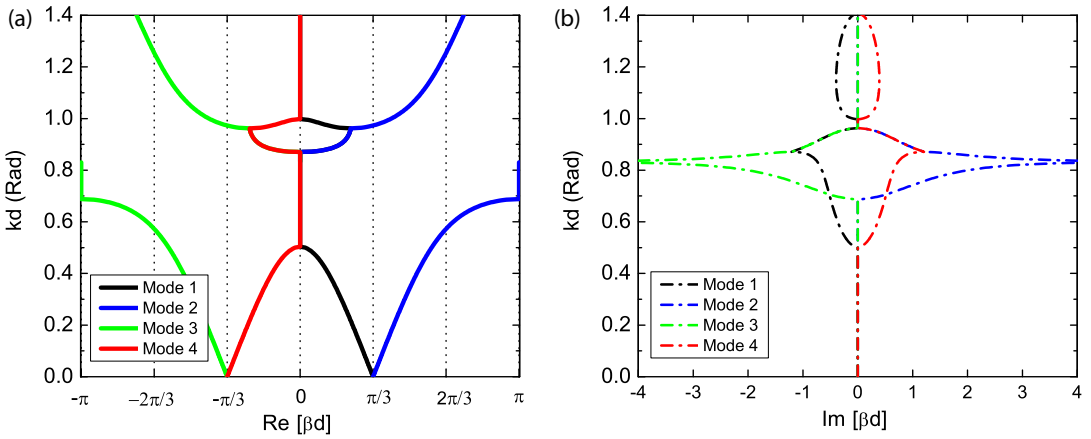

FIG. 2. (Color online) (a) The real and (b) the imaginary parts of the wave number of a twisted array composed of PEC dipoles. The angle of rotation between consecutive metasurfaces is $\pi/3$ rad, and the distance between consecutive metasurfaces is $d = 85$ nm. Solid and dashed lines refer to real and imaginary parts of the wave number, respectively. Real and imaginary parts of each mode have the same color. Around $kd = 0.9$ the metamaterial supports a pair of complex modes.

composed of PEC rods with dimensions $300 \times 50 \times 50$ nm in a square lattice with transverse periods equal to 350 nm in both directions. The transfer matrix of this metasurface is obtained using full-wave numerical simulations [57], and we initially assume an angle of rotation $\theta = \pi/3$ rad and $d = 85$ nm.

By using the numerically evaluated transfer matrix in Eq. (3), the dispersion diagram for the twisted metamaterial is easily calculated and is shown in Fig. 2. In general, four modes are supported by this structure, although at certain frequencies one or both pairs can have an imaginary part. The real and imaginary parts of the wave numbers, as obtained from (3), are shown with solid and dashed lines in panels (a) and (b), respectively. These diagrams are a bit unusual to read: For instance, the dispersion curves meet at $\beta d = \pm\pi/3$ for $kd = 0$, where k is the wave number in the background medium. The value of βd at zero frequency coincides with the rotation angle between two consecutive metasurfaces. This is a general property of the dispersion diagram for periodically twisted structures, which can be justified by the fact that at zero frequency the admittance of the metasurface is negligible, or equivalently the transfer matrix $\underline{\underline{\mathbf{T}}} = \underline{\underline{\mathbf{I}}}$ (with $\underline{\underline{\mathbf{I}}}$ being the identity matrix), implying that the eigensolution to (3) reduces to the eigenvalues of the rotation matrix, which are $e^{\pm i\theta}$. Thus the propagation constant β at frequencies near zero approaches the rotation angle divided by the length of the twisted unit cell (i.e., $\beta = \pm\theta/d$).

At sufficiently low frequencies all modes have real wave numbers, provided that the admittance [58] of the metasurface is sufficiently small as in our scenario. As the frequency increases, the propagation constants start to diverge from each other: The second and fourth modes (blue and red lines) have a positive slope, whereas the first and third modes (black and green lines) have a negative slope in the $\beta d - kd$ plane, corresponding as shown in the following to forward and backward modes, respectively. At sufficiently low frequencies the modal dispersion varies linearly with frequency as expected since the Taylor expansion of the transfer matrix can be written as $\underline{\underline{\mathbf{T}}} \approx \underline{\underline{\mathbf{I}}} + k\,\underline{\underline{\mathbf{T}}}'(0)$, where $\underline{\underline{\mathbf{T}}}'(0)$ is the derivative of the transfer matrix with respect to the free-space wave number at $k = 0$. Interestingly, the slope of this linear portion of the dispersion diagram is independent of the rotation angle. Around $kd = 0.5$, two of the modes reach the $\beta d = 0$ axis and become evanescent, and the structure supports only a pair of propagating modes in the frequency range of $0.5 < kd < 0.7$. At higher frequencies, this pair reaches the stop-band condition $\beta d = \pi$ and gains an imaginary part, and the structure exhibits a full band gap for which no propagation exists. For kd between 0.9 and 1.0, the twisted metamaterial supports four complex modes. These modes are more sensitive to the array parameters, compared to propagating or evanescent modes. For example, they are not supported if the distance between twisted unit cells increases from 85 to 95 nm. However, for smaller values of d, complex modes still exist in the structure. At $kd \sim 1.0$, these complex modes split into four propagating modes, two of which rapidly become evanescent at higher frequencies. Interestingly, band diagrams, such as the one in Fig. 2, may be plotted for arbitrary rotation angles and separation distance between neighboring metasurfaces, even in the case of strictly nonperiodic arrays, i.e., when 2π is not a multiple of the rotation angle.

In this context, it may be easily verified that (3) reduces to the case of a conventional periodic metamaterial if the rotation angle is zero or 2π since $\underline{\underline{\mathbf{R}}} = \underline{\underline{\mathbf{I}}}$. When $\underline{\underline{\mathbf{R}}}^N = \underline{\underline{\mathbf{I}}}$, which means the Nth metasurface has the same orientation as the metasurface at the origin, the twisted metamaterial becomes periodic, and it has a superlattice with periodicity $d' = Nd$. For this subclass of twisted metamaterials, our analytical results can be compared to band diagrams obtained from full-wave numerical simulations for conventional periodic structures. Since the length of the unit cell is different in these two approaches, the dispersion diagram of the twisted metamaterial based on (3) should be folded in an appropriate way to reproduce the conventional dispersion diagram of a periodic structure. For example, the propagation constant in the twisted metamaterial discussed in the example of Fig. 2 is related to the propagation constant in a corresponding periodic structure through the formula,

$$\beta' d' = 3\beta d \pm \pi, \tag{4}$$

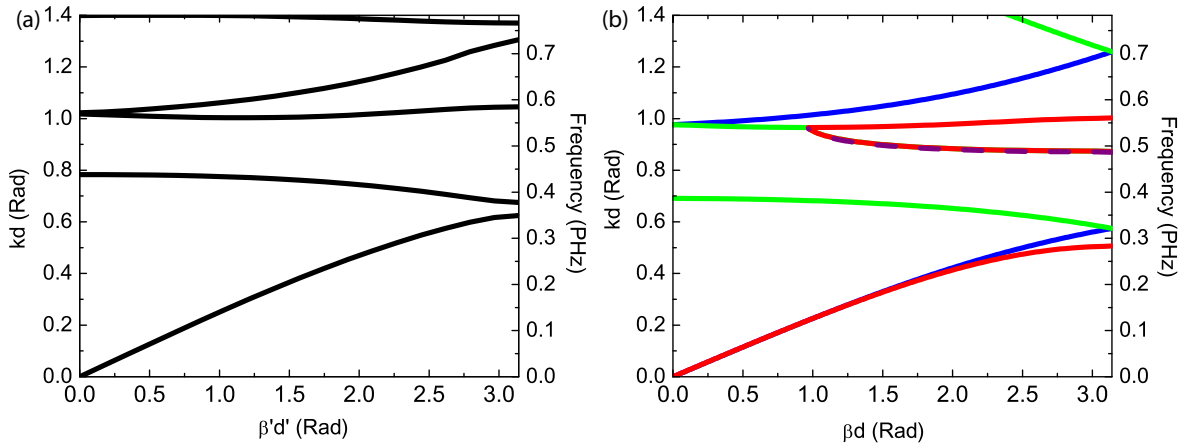

FIG. 3. (Color online) The dispersion diagram of a twisted metamaterial with supercell periodicity consisting of three twisted unit cells in the direction of propagation. (a) Dispersion diagram obtained from numerical simulations, and (b) analytical results obtained from (4). The real part of the complex modes is highlighted with purple.

where d' and β' are the lattice and the propagation constants in the periodic structure, respectively. The addition of π is due to the fact that three rotations in this twisted structure result in a rotation equal to π, but because of the inclusion symmetry (nanorods), this rotation is enough to produce a periodic supercell.

Based on this property, a supercell of the considered twisted metamaterial was simulated using full-wave simulations, and in Fig. 3 the simulation results [panel (a)] are compared with our analytical solution [panel (b)] after proper folding of the dispersion diagram of Fig. 2. For simplicity, we only plot the real part of $\beta' d'$ in Fig. 3(b) since our full-wave simulations cannot compute evanescent modes. The colors in panel (b) directly correspond to the different modes in Fig. 2. It is seen that our analytical solutions agree very well with the numerical simulations, especially at lower frequencies, validating our analysis. In this supercell representation, the dispersion relation starts at zero, as usual. At lower frequencies, two forward modes exist [modes 2 (red) and mode 4 (blue)]. As the propagation constant of these two modes crosses π/d' (i.e., $\beta' d' \rightarrow \pi$), they become evanescent and mode 3 (green) enters the range between zero and π/d'.

Our numerical simulations confirm that no propagating mode is supported in the frequency range of $0.8 < kd < 1.0$. This frequency gap corresponds to the stop band where only evanescent modes exist. Based on our analytical results, this stop band starts at $kd \approx 0.7$ instead of 0.8 as predicted by numerical simulations. In addition, some band gaps in the numerical simulations are not present in the analytical results when $\beta' d'$ approaches π. These minor discrepancies between full-wave numerical simulations and analytical results become more prominent when the phase shift between consecutive layers in the twisted structure becomes larger. For example, mode 4 (red line) reaches $\beta' d' = \pi$ at $kd \approx 0.5$, which corresponds to the phase shift $\beta d = 0$ in the dispersion diagram of Fig. 2. In this case, the difference between analytical and numerical results is relatively small. However, at a slightly higher frequency, modes 2 and 3 (blue and green lines) approach $\beta' d' = \pi$, which corresponds to $\beta d = \pm 2\pi/3$, and the discrepancy in this case becomes larger. Mode 3 (green line) approaches $\beta' d' = 0$ at $kd \approx 0.7$, which corresponds to $\beta d = -\pi$, and the discrepancy is the largest at this point. Similar observations can be extended to even higher frequencies. Therefore, it can be stated that larger discrepancies between numerical simulations and our analytical results occur at large values of βd. These observations are partially related to the fact that the thickness of the metasurface composing the twisted metamaterial is not zero as assumed in the analytical solution, in fact it is comparable to the distance between metasurfaces. For larger phase shifts, the phase error due to neglecting the finite size of metasurfaces is larger; therefore it is responsible for the larger discrepancies between full-wave simulations and the analytical model.

It is worth noting that, in our analytical results, an additional dispersion curve (the red curve with purple dashed highlights) arises in this stop band. This additional curve is associated with the complex mode evolved from mode 4, which is not captured by our full-wave simulations limited to only purely real propagation constants. At higher frequencies ($kd > 1$), some discrepancy between the numerical and the analytical solution arises, associated with the fact that the metasurface can no longer be homogenized with the surface impedance model used in our analytical calculations because the wavelength is comparable to the transverse periodicity of the metasurface. This may be easily corrected with an extended analytical approach that takes into account more than one transverse Floquet harmonics in (3). In addition, the small discrepancy between a rotated metasurface as considered in our theory and a metasurface with rotated inclusions but the same lattice as the one considered in our numerical simulations becomes more pronounced at higher frequencies [54].

III. POLARIZATION PROPERTIES OF THE EIGENMODES

Our theory can also easily highlight and provide insight into the polarization properties of the eigenmodes derived in the previous section. To this end, we decompose the electric field propagating in the twisted structure into the superposition of right-handed and left-handed circularly polarized waves $[\mathbf{E} = (\hat{x} + i\hat{y})E_L + (\hat{x} - i\hat{y})E_R]$, where $\hat{x}$ and $\hat{y}$ are unit vectors along the x and y directions, respectively. This analysis

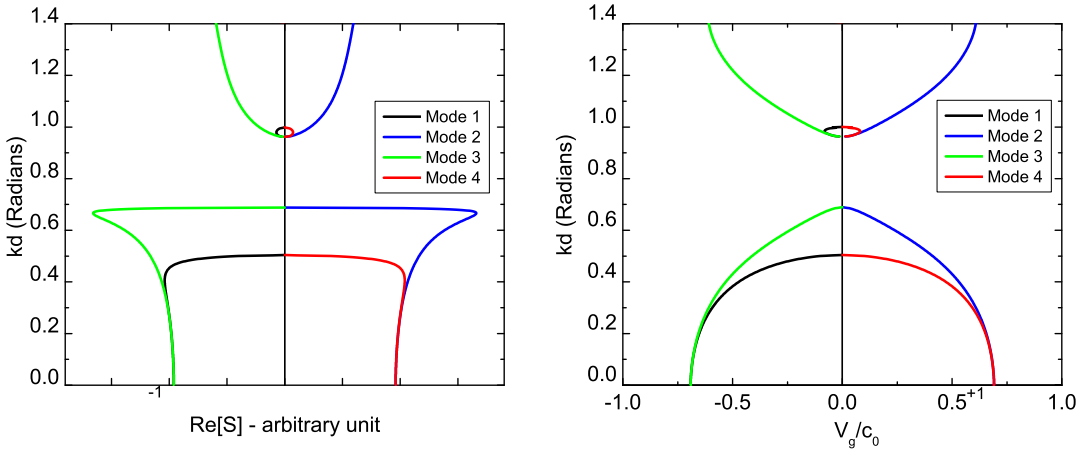

FIG. 4. (Color online) (a) Real part of the Poynting vector in the direction of propagation (Re[S_z]) as a function of wave number (k) for the same metamaterial as in previous figures. (b) Group velocity normalized to the speed of light in vacuum of the modes as a function of the wave number. Comparison between the figures reveals that both the group velocity and the Poynting vector show the same direction of energy propagation for different modes.

has several advantages: First, when only one mode exists, examining its polarization properties may result in optimal designs for polarization control. In addition, group velocity and Poynting vector distribution of the different modes can naturally be evaluated in this representation.

Since $\mathbf{E}_{n+1} = \underline{\underline{\mathbf{r}}}\mathbf{E}_n\, e^{i\beta d}$, where $\underline{\underline{\mathbf{r}}}$ is the 2×2 rotation matrix with angle of rotation θ, it is easy to prove that E_R and E_L for each eigenmode satisfy the equations,

$$E_{Rn+1} = E_{Rn}e^{i(\beta d-\theta)},$$
$$E_{Ln+1} = E_{Ln}e^{i(\beta d+\theta)}. \quad (5)$$

Therefore, right- and left-handed components are plane waves traveling with wave vectors equal to $\beta - \theta/d$ and $\beta + \theta/d$, respectively. It is important to note that the amplitudes of left- and right-handed terms are not independent, i.e., in general it is not possible to excite just one of these circularly polarized waves since the eigenmodes are not purely circularly polarized, and for each eigenmode the two components in (5) exchange power as they propagate along the array. However, as we discuss in the following, twisted metamaterials tend to naturally support eigenmodes with one of the circular polarizations significantly stronger than the other one, which justifies this representation. This is obviously of interest to develop optical devices that manipulate and filter light polarization [9]. Similar relations can be obtained for left- and right-handed components of the magnetic field.

For a twisted metamaterial made of lossless metasurfaces as the one considered here for simplicity, the wave number can be real (for propagating modes), purely imaginary (for evanescent modes), or complex with a pair of modes supporting complex conjugate β as derived in Figs. 2 and 3. The Poynting vector can be defined for all these modes, and its real part Re S_z in the direction of propagation for the metamaterial of Figs. 2 and 3 is shown in Fig. 4(a). Here the Poynting vector is plotted for normalized modes [the norm of the field vector $\mathbf{f}$ in (3) being set to 1]. At lower frequencies, one of the modes has a negative propagation constant and positive Re[S_z] (mode 1, black line in the figures), which shows that the energy travels opposite to the generalized Floquet phase. This does not imply that the mode is backward because the definition of the wave number β is different from the conventional definition in periodic structures as shown in (4). In fact, the fields defined in a reference frame at rest, such as in (5), do not have a unique phase velocity, but the left-handed and right-handed components appear to travel at different velocities. However, using (5) it is possible to uniquely define a group velocity for the modes: By assuming that the fields are slowly modulated in the direction of propagation, we can represent them as

$$\mathbf{E}(z) = E_L e^{i(\beta+\theta/d)z}(\hat{x} + i\,\hat{y}) + E_R e^{i(\beta-\theta/d)z}(\hat{x} - i\,\hat{y}), \quad (6)$$

and define the group velocity as $v_g = \partial\omega/\partial\beta$ for propagating modes, which is the same for both left- and right-handed components as shown in Fig. 4(b) [59]. The group velocity confirms the direction of propagation of all modes, consistent with the Poynting vector in Fig. 4(a). As mentioned earlier, the slope of the dispersion diagram in Fig. 2 does not depend on the rotation angle at low frequencies. This implies that the group velocity also is independent of the rotation angle at low frequencies. As the frequency increases, the modes approach the first cutoff, and the group velocity correspondingly approaches zero. An interesting feature of the Poynting vector distribution is a maximum of power flow for modes 2 and 3 right before the first stop band, associated with a large increase in stored energy. The energy velocity, consistent with the group velocity shown in Fig. 4(b), converges smoothly to zero towards the stop band, but the increase in stored energy in these modes implies a large power flow.

The representation of eigenmodes in terms of circularly polarized waves allows us to analyze the polarization evolution of each mode, shown in Fig. 5. The figure shows the logarithm of the ratio $|E_L|/|E_R|$ for all propagating modes in the same format as Fig. 2. At very low frequencies, each mode is strongly circularly polarized. Modes 1 (black) and 2 (blue) are polarized as $\hat{x} + i\,\hat{y}$, and modes 3 (green) and 4 (red) are polarized as $\hat{x} - i\,\hat{y}$, which, combined with the propagation direction extracted in the previous analysis, indicates that modes 1 and 4 are right-handed circularly polarized and modes 2 and 3 are left-handed circularly polarized. Notice that in the

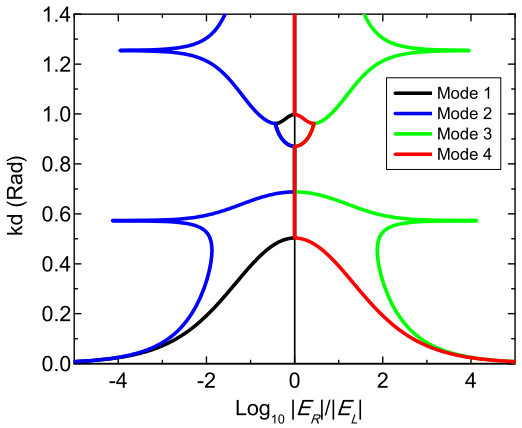

FIG. 5. (Color online) The evolution of polarization properties for the eigenmodes of Figs. 2–4 [defined as the logarithm of the ratio of left- to right-handed components ($\log_{10}|E_L|/|E_R|$)] as a function of frequency. In some frequency bands, only one pair of propagating modes with approximately circular polarization exists.

low-frequency limit the interaction with the metasurfaces is very weak, and in practice we have only two linearly polarized modes propagating in the background medium, the linear combination of the degenerate circularly polarized modes described in our theory. As the frequency increases, these modes split, and their circular polarization properties become less strong. Finally, they become linearly polarized modes at the stop band. Modes 2 and 3 more strongly retain their circular polarization properties at the special point $kd \sim 0.6$, before converging to the band gap. It is possible to prove, inspecting Eqs. (3)–(6), that this special frequency point with a large circular polarization signature corresponds to the situation when the phase shift between two neighboring metasurfaces (βd) is exactly equal to $\pi - \theta$ or $-\pi + \theta$. A similar response is also observed at $kd \sim 1.25$ for modes 3 and 4 (green and red lines) since the phase shift for these modes becomes $\pi - \theta$ or $-\pi + \theta$.

Since the horizontal axis of Fig. 5 is logarithmic, it is clear that the modes supported by the twisted metamaterial retain a high degree of circular polarization for a large part of their bandwidth of propagation. In the single-mode regime ($0.43 < kd < 0.68$ and $1.0 < kd < 1.4$), in particular, where there is only one forward propagating mode, this high degree of circular polarization can be exploited to design effective circular polarizers for electromagnetic waves. More specifically, if a slab of twisted metamaterial is illuminated by a plane wave in this single-mode frequency range, only one circularly polarized mode is excited and transmitted through the structure. Using our analytical approach, we can efficiently optimize the rotation angle, the distance between metasurfaces, and the resonant properties of the inclusions to tailor the stop band and single-mode bandwidth and create optimal broadband circular polarizers in this planarized geometry.

IV. EXCITATION OF TWISTED METAMATERIALS

The reflection and transmission coefficients of a plane wave normally incident on the interface of a half-space or a slab of twisted metamaterial can be found using the continuity of tangential fields at the boundary and assuming that the fields inside the twisted metamaterial can be represented as in (6). A sketch of this scattering problem is shown in Fig. 6(a). In the case of scattering from the half-space, we need to consider only eigenmodes carrying power in the positive direction, i.e., away from the interface, which are easily determined in Fig. 4. Given the natural description of eigenmodes in terms of circularly polarized modes, here we calculate the reflection coefficients for right- and left-handed plane waves impinging on a half-space filled with the twisted metamaterial of Fig. 2 using this analytical approach as shown in Fig. 6(b). Here, R_{RL} represents the reflection coefficient for the left-handed circularly polarized incidence and the right-handed circularly polarized reflected wave and similarly for the other coefficients. Different bands can be identified in this figure, consistent with the eigenmodal results shown in the previous figures: At lower frequencies, both polarizations penetrate the structure and, therefore, the reflection coefficients have small values. In this regime, the structure is impedance matched to the free space because the metasurfaces have a

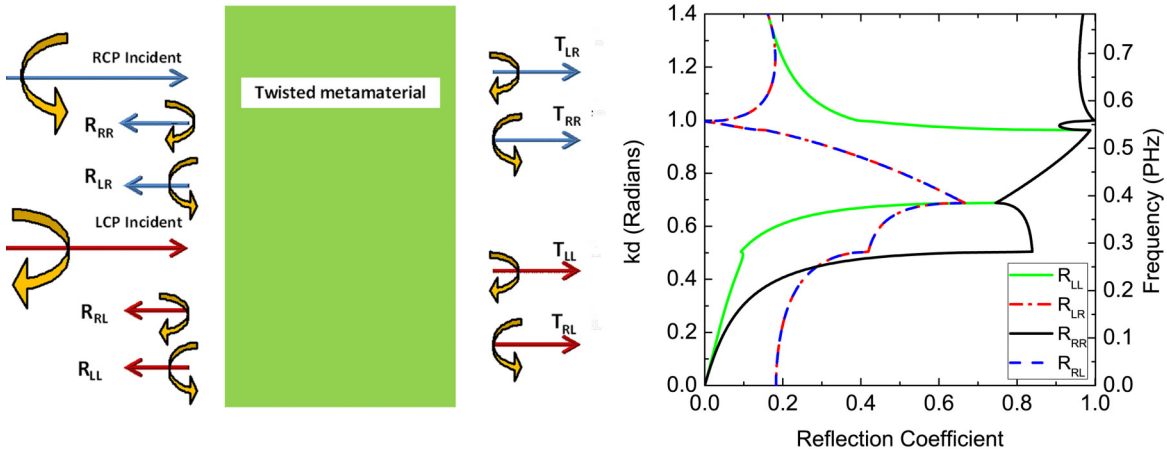

FIG. 6. (Color online) (a) The excitation setup and scattering coefficients for scattering from a slab. In the case of scattering from the half-space the width of the twisted material slab approaches infinity. (b) Reflection coefficients from a half-space composed of the twisted array of Fig. 2 calculated using the analytical formulation developed in this paper.

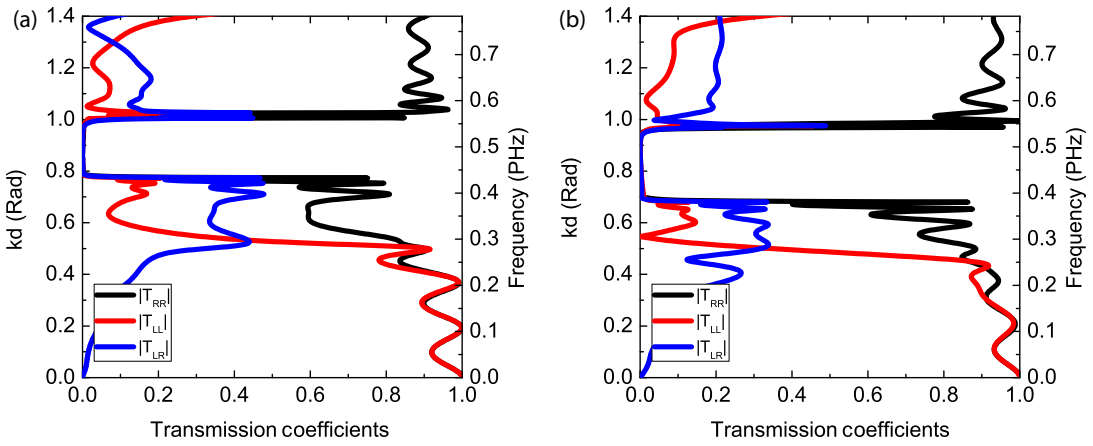

FIG. 7. (Color online) Transmission coefficients for a slab of twisted metamaterial with a total thickness of 1 μm. (a) Full-wave numerical simulations and (b) analytical results.

weak interaction with the wave and we assumed a free-space background between them. When the frequency increases, the reflection coefficients grow, consistent with the different modal dispersions for different polarizations. In the frequency band with single eigenmode propagation ($0.43 < kd < 0.68$ and $1.0 < kd < 1.4$) for which the propagating mode has a strong right-handed polarization, right-handed plane waves penetrate the half-space, whereas left-handed waves are completely reflected. In the stop band, both polarizations are reflected, and no propagating wave can be transmitted in the metamaterial. The imparted rotation in the structure controls the transmission of the left- or right-handed waves. Notice in the figure how, due to the symmetry of the inclusions $R_{\mathrm{RL}} = R_{\mathrm{LR}}$, these polarization coupling coefficients are not negligible, especially in the band-gap region.

This analysis can also be extended to evaluate the transmission and reflection from a slab of twisted metamaterial with finite thickness. Due to the reflections at the second interface, here all four modes in the metamaterial are excited, and it is not necessary to distinguish between forward and backward propagating modes. The transmission coefficients for left- and right-handed waves are shown in Fig. 7, where T_{LL} (T_{RR}) is the transmission coefficients of the left-handed (right-handed) circularly polarized waves when the incident wave has the same polarization. T_{LR} is the transmission coefficient of the left-handed circular waves when excited with right-handed circular polarization. Again, T_{LR} and T_{RL} are equal to each other in this case and, therefore, only one of them is shown. In our analytical results [panel (a)], we consider the same twisted metamaterial as in the previous analysis but with a finite thickness of 1 μm. For comparison, we also show the transmission coefficients calculated with full-wave simulations [panel (b)]. Similar bands in the frequency response of the slab can be identified as in Fig. 6, proving the effectiveness of the approach presented here and of the use of this thin planarized metamaterial as a broadband circular polarizer. In the single-mode frequency ranges, the slab acts as a broadband circular polarizer, filtering one circular polarization from the incident fields, whereas in other frequency ranges either both modes pass through the slab or none of the modes can penetrate the twisted structure. It is remarkable how this thin structure, formed by fully achiral inclusions, allows opening significant bands with large polarization selection, based on the combination of the resonant response of the nanorods and their sequential rotation within the lattice.

V. CONCLUSIONS

In this paper, we have developed a generalized Bloch analysis that efficiently characterizes the modal dispersion in a twisted 3D array of periodic structures. This method is based on the assumption that each metasurface forming the array can be modeled using a transfer matrix with negligible near-field coupling between layers, an assumption that has been shown to hold well in the considered examples, validated with full-wave simulations. Using this approach, it is possible to obtain the eigenmodes supported by a twisted metamaterial, including evanescent and complex modes. Our analysis also allows studying and efficiently optimizing the polarization evolution of these modes in the different propagation bands, and it sheds insight into how the sequential rotation along the lattice introduces a preferred circularly polarized nature for the propagating modes in the structure. By controlling the twist angle and metasurface design, we can develop optimized passband and stop-band features with desired polarization selectivity for planarized ultrathin nanophotonic devices based on stacked metasurfaces.

ACKNOWLEDGMENTS

This work was supported by the Air Force Office of Scientific Research with Grant No. FA9550-13-1-0204, by the Office of Naval Research with MURI Grant No. N00014-10-1-0942, and by the Welch foundation with Grant No. F-1802.

APPENDIX: TRANSFER MATRIX DERIVATION AND ITS PROPERTIES

We define the transfer matrix of a metasurface in the presence of transverse electromagnetic waves as

$$\begin{bmatrix} \mathbf{F}_2 \\ \mathbf{L}_2 \end{bmatrix} = \underline{\underline{\mathbf{T}}} \begin{bmatrix} \mathbf{F}_1 \\ \mathbf{L}_1 \end{bmatrix}, \tag{A1}$$

where $\mathbf{F}$ and $\mathbf{L}$ are defined as

$$\mathbf{F} = \begin{bmatrix} E_y \\ H_x \end{bmatrix}, \tag{A2}$$

$$\mathbf{L} = \begin{bmatrix} E_x \\ H_y \end{bmatrix}, \tag{A3}$$

and the subscripts 1 and 2 refer to the input and output sides of the unit cell.

$\underline{\underline{\mathbf{T}}}$ is a 4×4 transfer matrix which can be partitioned into four 2×2 blocks $\underline{\underline{\mathbf{A}}}$, $\underline{\underline{\mathbf{B}}}$, $\underline{\underline{\mathbf{C}}}$, and $\underline{\underline{\mathbf{D}}}$. For a purely imaginary impedance matrix, corresponding to a lossless metasurface, it is easy to prove that the diagonal terms of $\underline{\underline{\mathbf{A}}}$, $\underline{\underline{\mathbf{B}}}$, $\underline{\underline{\mathbf{C}}}$, and $\underline{\underline{\mathbf{D}}}$ are real valued and the off-diagonal terms are purely imaginary. This condition is necessary but not sufficient for a transfer matrix $\underline{\underline{\mathbf{T}}}$ to represent a lossless unit cell of our twisted metamaterial geometry. In order to have a lossless transfer matrix the following conditions should also be satisfied:

$$\det \underline{\underline{\mathbf{A}}} - \det \underline{\underline{\mathbf{C}}} = 1, \tag{A4}$$

$$\det \underline{\underline{\mathbf{B}}} - \det \underline{\underline{\mathbf{D}}} = -1, \tag{A5}$$

$$\mathrm{adj}(\underline{\underline{\mathbf{B}}}) \cdot \underline{\underline{\mathbf{A}}} = \mathrm{adj}(\underline{\underline{\mathbf{D}}}) \cdot \underline{\underline{\mathbf{C}}}, \tag{A6}$$

where $\mathrm{adj}(\cdot)$ stands for the adjoint operation on a matrix. Equation (A6) can also be written in the following equivalent form:

$$\mathrm{adj}(\underline{\underline{\mathbf{A}}}) \cdot \underline{\underline{\mathbf{B}}} = \mathrm{adj}(\underline{\underline{\mathbf{C}}}) \cdot \underline{\underline{\mathbf{D}}}. \tag{A7}$$

The above equations are obtained by equating input and output powers of the transfer matrix.

For a reciprocal transfer matrix we also have

$$\det \underline{\underline{\mathbf{T}}} = 1. \tag{A8}$$

Since the determinant equals the product of all eigenvalues, Eq. (A8) ensures that for a reciprocal unit cell the sum of all wave numbers is necessarily zero.

In order to derive the properties of the eigensolutions of Eq. (3) for $n = 0$, we alter the definition of the transfer matrix using the auxiliary vectors,

$$\mathbf{F}' = \mathbf{E} = \begin{bmatrix} E_x \\ E_y \end{bmatrix}, \quad \mathbf{L}' = \mathbf{H} = \begin{bmatrix} H_x \\ H_y \end{bmatrix}. \tag{A9}$$

With these new definitions, the condition on the $\underline{\underline{\mathbf{A}}}$, $\underline{\underline{\mathbf{B}}}$, $\underline{\underline{\mathbf{C}}}$, and $\underline{\underline{\mathbf{D}}}$ elements being purely real or purely imaginary for a lossless metasurface translates into the following condition on $\underline{\underline{\mathbf{A}}}'$, $\underline{\underline{\mathbf{B}}}'$, $\underline{\underline{\mathbf{C}}}'$, and $\underline{\underline{\mathbf{D}}}'$:

$$\underline{\underline{\mathbf{A}}}' = \underline{\underline{\mathbf{A}}}'^{*}, \quad \underline{\underline{\mathbf{B}}}' = -\underline{\underline{\mathbf{B}}}'^{*}, \quad \underline{\underline{\mathbf{C}}}' = -\underline{\underline{\mathbf{C}}}'^{*}, \quad \underline{\underline{\mathbf{D}}}' = \underline{\underline{\mathbf{D}}}'^{*}. \tag{A10}$$

It is easy to show that Eq. (A10) is equivalent to requiring that the metasurface satisfies time-reversal symmetry. With these definitions, Eqs. (A4)–(A7) become more complex, thus it is reasonable to use the two different definitions to study different aspects of the transfer matrix.

The eigensystem (3) for $n = 0$ is

$$(\underline{\underline{\mathbf{T}}}' - e^{i\beta d}\underline{\underline{\mathbf{R}}}) \begin{bmatrix} \mathbf{E} \\ \mathbf{H} \end{bmatrix} = 0. \tag{A11}$$

In the above equation $\underline{\underline{\mathbf{R}}}$ is the 4×4 rotation matrix defined as

$$\underline{\underline{\mathbf{R}}} = \begin{bmatrix} \underline{\mathbf{r}} & 0 \\ 0 & \underline{\mathbf{r}} \end{bmatrix}, \tag{A12}$$

where $\underline{\mathbf{r}}$ is the 2×2 rotation matrix in the Cartesian coordinate system [61]. By replacing the transfer matrix with its block constituents and using Eq. (A12) in Eq. (A11), we obtain

$$\begin{aligned} \underline{\underline{\mathbf{A}}}'\mathbf{E} + \underline{\underline{\mathbf{B}}}'\mathbf{H} &= e^{i\beta d}\underline{\mathbf{r}}\mathbf{E}, \\ \underline{\underline{\mathbf{C}}}'\mathbf{E} + \underline{\underline{\mathbf{D}}}'\mathbf{H} &= e^{i\beta d}\underline{\mathbf{r}}\mathbf{H}. \end{aligned} \tag{A13}$$

Assuming that there is a set of fields ($\mathbf{E}$ and $\mathbf{H}$) and a wave number β satisfying the above equations for a transfer matrix satisfying condition (A10), the following equations also hold true:

$$\begin{aligned} \underline{\underline{\mathbf{A}}}'\mathbf{E}^* - \underline{\underline{\mathbf{B}}}'\mathbf{H}^* &= e^{-i\beta^* d}\underline{\mathbf{r}}\mathbf{E}^*, \\ \underline{\underline{\mathbf{C}}}'\mathbf{E}^* - \underline{\underline{\mathbf{D}}}'\mathbf{H}^* &= -e^{-i\beta^* d}\underline{\mathbf{r}}\mathbf{H}^*. \end{aligned} \tag{A14}$$

Equation (A14) shows that the field vectors $\mathbf{E}^*$ and $-\mathbf{H}^*$ are also eigensolutions of the structure with a wave number $-\beta^*$. Note that this result does not need the transfer matrix to be lossless but simply that it satisfies time-reversal symmetry.

An important set of relations between the block matrices can also be found if we assume reflection symmetry for each metasurface, an assumption that always holds for ultrathin metasurfaces. By applying this symmetry operation, we are able to show the relations,

$$\begin{aligned} \underline{\underline{\mathbf{A}}}'\underline{\underline{\mathbf{A}}}' - \underline{\underline{\mathbf{B}}}'\underline{\underline{\mathbf{C}}}' &= \underline{\mathbf{I}}, \\ \underline{\underline{\mathbf{C}}}'\underline{\underline{\mathbf{A}}}' - \underline{\underline{\mathbf{D}}}'\underline{\underline{\mathbf{C}}}' &= 0, \\ \underline{\underline{\mathbf{A}}}'\underline{\underline{\mathbf{B}}}' - \underline{\underline{\mathbf{B}}}'\underline{\underline{\mathbf{D}}}' &= 0, \\ \underline{\underline{\mathbf{D}}}'\underline{\underline{\mathbf{D}}}' - \underline{\underline{\mathbf{C}}}'\underline{\underline{\mathbf{B}}}' &= \underline{\mathbf{I}}, \end{aligned} \tag{A15}$$

which in turn confirm that two twisted arrays with an opposite sense of rotations have the same modal solutions. A forward propagating mode in one structure resembles the backward propagating mode in the other array. Explicitly, we can write

$$\begin{aligned} \beta^+ &= -\beta^-, \\ \mathbf{E}^+_{n+1} &= \mathbf{E}^-_{-n}, \\ \mathbf{H}^+_{n+1} &= -\mathbf{H}^-_{-n}, \end{aligned} \tag{A16}$$

where the superscripts point to a positive or negative sense of rotation between two consecutive metasurfaces in the twisted array.

[1] T. A. Morgado, J. S. Marcos, S. I. Maslovski, and M. G. Silveirinha, Appl. Phys. Lett. **101**, 021104 (2012).

[2] R. A. Brazhe and R. M. Meftakhutdinov, Tech. Phys. **52**, 793 (2007).

[3] H.-H. Huang and Y.-C. Hung, Proc. SPIE **8632**, 863222 (2013).

[4] J. Nemirovsky, M. C. Rechtsman, and M. Segev, Opt. Express **20**, 8907 (2012).

[5] A. Demetriadou and J. B. Pendry, J. Phys.: Condens. Matter **21**, 376003 (2009).

[6] E. Plum, J. Zhou, J. Dong, V. A. Fedotov, T. Koschny, C. M. Soukoulis, and N. I. Zheludev, Phys. Rev. B **79**, 035407 (2009).

[7] J. B. Pendry, Science **306**, 1353 (2004).

[8] A. A. Zharov, N. A. Zharova, R. E. Noskov, I. V. Shadrivov, and Y. S. Kivshar, New J. Phys. **7**, 220 (2005).

[9] Y. Zhao, M. A. Belkin, and A. Alù, Nat. Commun. **3**, 870 (2012).

[10] L. Wu, Z. Yang, Y. Cheng, Z. Lu, P. Zhang, M. Zhao, R. Gong, X. Yuan, Y. Zheng, and J. Duan, Opt. Express **21**, 5239 (2013).

[11] A. Christofi, N. Stefanou, G. Gantzounis, and N. Papanikolaou, J. Phys. Chem. C **116**, 16674 (2012).

[12] M. Decker, R. Zhao, C. M. Soukoulis, S. Linden, and M. Wegener, Opt. Lett. **35**, 1593 (2010).

[13] M. Decker, M. Ruther, C. E. Kriegler, J. Zhou, C. M. Soukoulis, S. Linden, and M. Wegener, Opt. Lett. **34**, 2501 (2009).

[14] H. Liu, D. A. Genov, D. M. Wu, Y. M. Liu, Z. W. Liu, C. Sun, S. N. Zhu, and X. Zhang, Phys. Rev. B **76**, 073101 (2007).

[15] B. Bai, Y. Svirko, J. Turunen, and T. Vallius, Phys. Rev. A **76**, 023811 (2007).

[16] A. Andryieuski, C. Menzel, C. Rockstuhl, R. Malureanu, F. Lederer, and A. Lavrinenko, Phys. Rev. B **82**, 235107 (2010).

[17] A. V. Rogacheva, V. A. Fedotov, A. S. Schwanecke, and N. I. Zheludev, Phys. Rev. Lett. **97**, 177401 (2006).

[18] M. Mitov and N. Dessaud, Nature Mater. **5**, 361 (2006).

[19] Y. Hadad and B. Z. Steinberg, Opt. Express **21**, A77 (2012).

[20] M. Ozaki, Y. Matsuhisa, H. Yoshida, R. Ozaki, and A. Fujii, Phys. Status Solidi A **204**, 3777 (2007).

[21] A. H. Gevorgyan and M. Z. Harutyunyan, Phys. Rev. E **76**, 031701 (2007).

[22] J. Costa and M. Silveirinha, Opt. Express **20**, 13915 (2012).

[23] C. Menzel, C. Helgert, C. Rockstuhl, E.-B. Kley, A. Tünnermann, T. Pertsch, and F. Lederer, Phys. Rev. Lett. **104**, 253902 (2010).

[24] Y. Tang and A. E. Cohen, Science **332**, 333 (2011).

[25] Y. Tang and A. E. Cohen, Phys. Rev. Lett. **104**, 163901 (2010).

[26] G. G. Denisov, V. L. Bratman, A. W. Cross, W. He, A. D. R. Phelps, K. Ronald, S. V. Samsonov, and C. G. Whyte, Phys. Rev. Lett. **81**, 5680 (1998).

[27] S. J. Cooke and G. G. Denisov, IEEE Trans. Plasma Sci. **26**, 519 (1998).

[28] G. G. Denisov, V. L. Bratman, A. D. R. Phelps, and S. V. Samsonov, IEEE Trans. Plasma Sci. **26**, 508 (1998).

[29] G. Shvets, Appl. Phys. Lett. **89**, 141127 (2006).

[30] K. J. Bunch, R. W. Grow, and J. M. Baird, Int. J. Infrared. Milli. **9**, 609 (1988).

[31] A. Alù, Phys. Rev. B **83**, 081102(R) (2011).

[32] C. R. Simovski, J. Opt. **13**, 013001 (2011).

[33] R. A. Shore and A. D. Yaghjian, Radio Sci. **47**, RS2014 (2012).

[34] Campione *et al.*, Photon. Nanostruct. Fund. Appl. **11**, 423 (2013).

[35] H. L. Ong and R. B. Meyer, J. Opt. Soc. Am. A **2**, 198 (1985).

[36] H. L. Ong, J. Appl. Phys. **64**, 614 (1988).

[37] P. McIntyre, J. Opt. Soc. Am. **68**, 869 (1978).

[38] P. McIntyre and A. W. Snyder, J. Opt. Soc. Am. **68**, 149 (1978).

[39] R. M. A. Azzam and N. M. Bashara, J. Opt. Soc. Am. **62**, 1252 (1972).

[40] F. Di Pasquale, F. A. Fernandez, S. E. Day, and J. B. Davies, IEEE J. Sel. Top. Quantum Electron. **2**, 128 (1996).

[41] D. Van Orden and V. Lomakin, IEEE Trans. Antennas Propag. **59**, 2824 (2011).

[42] D. Van Orden, Y. Fainman, and V. Lomakin, Opt. Lett. **35**, 2579 (2010).

[43] D. W. Berreman, J. Opt. Soc. Am. **62**, 502 (1972).

[44] D. W. Berreman, J. Opt. Soc. Am. **63**, 1374 (1973).

[45] R. J. Gagnon, J. Opt. Soc. Am. **71**, 348 (1981).

[46] H. Wöhler, G. Haas, M. Fritsch, and D. A. Mlynski, J. Opt. Soc. Am. A **5**, 1554 (1988).

[47] M. Foresti, J. Opt. Soc. Am. A **6**, 1254 (1989).

[48] C. Oldano, Phys. Rev. A **40**, 6014 (1989).

[49] E. Georgieva, J. Opt. Soc. Am. A **12**, 2203 (1995).

[50] A. Lakhtakia and W. S. Weiglhofer, Proc. R. Soc. A **448**, 419 (1995).

[51] E. V. Aksenova, A. A. Karetnikov, A. P. Kovshik, E. V. Kryukov, and V. P. Romanov, J. Opt. Soc. Am. A **25**, 600 (2008).

[52] H. de Vries, Acta Crystallogr. **4**, 219 (1951).

[53] Strictly speaking, $\underline{\underline{\mathbf{RTR}}}^{-1}$ is the transfer matrix of a rotated metasurface. However, as shown in Ref. [54], the transfer matrix of a metasurface with rotated inclusions and fixed lattice arrangement as the ones considered in our full-wave simulations has a small difference compared to the transfer matrix of a rotated metasurface for long wavelengths.

[54] Y. Zhao, N. Engheta, and A. Alù, Metamaterials **5**, 90 (2011).

[55] W. N. Cain and R. W. Grow, Int. J. Infrared. Milli. **10**, 1289 (1989).

[56] A. A. Barybin, Prog. Electromagn. Res. **19**, 241 (1998).

[57] CST of America, Inc., CST MICROWAVE STUDIO™ (CST, San Mateo, CA, 2012).

[58] The admittance is related to the transfer-matrix elements as explained in Ref. [54]. For example $Y_{yy} = \frac{-2}{\eta_0}(1 + \frac{T_{xx}}{T_{xy}T_{yx} - T_{xx}T_{yy}})$ where the elements of the transfer matrix are specified using appropriate subscripts.

[59] In Fig. 4(b) we do not show the group velocity for complex modes since it loses its physical meaning and it may assume values even larger than the velocity of light in free space c_0. A discussion of different complications arising from considering group velocity in complex wave numbers can be found in Ref. [60] and references therein, and it applies to periodic arrays as much as to twisted structures.

[60] P. Y. Chen, R. C. McPhedran, C. M. de Sterke, C. G. Poulton, A. A. Asatryan, L. C. Botten, and M. J. Steel, Phys. Rev. A **82**, 053825 (2010).

[61] The 2×2 rotation matrix is given by $\underline{\underline{\mathbf{r}}} = \begin{bmatrix} \cos\theta & -\sin\theta \\ \sin\theta & \cos\theta \end{bmatrix}$.